Pressure Sintering of Micro-Silver Joints in SiC Power Devices: Optimization of Processing Parameters and FEM Analysis

Guang Yang[1] · Ee Lynn Lee[1,2] · Kai Yang[1] · Fengshun Wu[1] · Longzao Zhou[1] · Liguo Ding[3] · Kewei Li[3] · Xuemin Li[3]

Abstract

The sintering process of micro-silver joints in SiC devices that operate in high temperatures has attracted considerable attention in recent years, owing to its advantages in low processing temperatures. The first part of this work carries out a thorough investigation into the effects of the processing parameters in pressure sintering on the shear strength and shear fracture surfaces of micro-silver joints. Optimization of the sintering parameters is then performed using orthogonal tests, validated by experiments, followed by an inspection of the microstructure of the sintered micro-silver joint. The second part of this work presents temperature and stress distribution analyses in the sintering process under the optimum parameters using the finite element method (FEM). The residual shear stress at the silver layer/SiC chip interface created during sintering is also examined. Results show that the shear strength of the silver joints increased significantly with the sintering temperature and time. The shear strength also increased with the sintering pressure initially, but a further increase in the sintering pressure (> 8 MPa) led to a decrease in the shear strength. Our findings demonstrate that the shear strength of the micro-silver joint may be correlated with the residual shear stress created during the sintering process. FEM showed that a further increase in sintering pressure resulted in an increase in residual shear stress, which reduced the shear strength. The optimum sintering parameters proposed for micro-silver joints based on these results are 290°C, 5 min, and 8 MPa, in which strong bonding strength of 44.31 MPa was achieved.

Keywords Micro-silver · pressure sintering · shear strength · FEM · residual shear stress

Introduction

With the rapid development of the electric vehicle industry, the requirements for power devices have become more stringent, such as operating under higher current density, temperature, and switching frequency.[1] However, the traditional Si-based semiconductor cannot fulfill these requirements.[2]

✉ Fengshun Wu
  fengshunwu@hust.edu.cn

✉ Longzao Zhou
  lzzhou@hust.edu.cn

1 School of Materials Science and Engineering, Huazhong University of Science and Technology, Wuhan 430074, China

2 Department of Mechanical Engineering, Faculty of Engineering, Universiti Malaya, 50603 Kuala Lumpur, Malaysia

3 Chengdu Silan Semiconductor Manufacturing Co., Ltd., Chengdu 610404, China

Thus, wide-bandgap semiconductor material SiC has been introduced owing to its outstanding properties.[3,4] The theoretical operating temperature of SiC can reach 600°C,[5] whereas the operating temperature of Si is about 200°C. The blocking voltage of a SiC-based insulated gate bipolar transistor (IGBT) is much higher than Si,[6] and the inverter composed of SiC-based metal–oxide–semiconductor field-effect transistor (MOSFET) has 20–30% higher efficiency than that of a Si-based equivalent.[7]

The conventional joint materials in Si-based IGBTs generally have lower melting points (~200°C) that limit the maximum working temperature. Given the capability of SiC to operate in higher temperatures and the differences between the material properties of SiC and Si, such as Young's modulus (E) and the coefficient of thermal expansion (CTE), the existing chip-to-substrate interconnects in Si-based devices are less suitable for SiC-based devices.[8] The existing interconnects that are used for high-temperature applications include transient liquid-phase (TLP) interconnects,[9,10] high-temperature solder interconnects (i.e.,

Pb-based solders and Au–Sn),[11,12] and nano-silver/copper or micro-silver/copper sintering interconnects.[13–15] Among these interconnects, nano-silver or micro-silver sintering interconnect joints demonstrate good development prospects due to the advantages of low processing temperature, promising properties of high-temperature application, good resistance to oxidation, good thermal conductivity, and good electrical conductivity.[4]

Various sintering processes with or without the application of pressure have been developed to produce sintered silver joints with promising qualities.[14–17] In general, pressure sintering can achieve a better densification in silver joints with particles of larger diameters. Although a larger particle requires higher sintering pressure and temperature that result in a higher manufacturing cost, the formulation of smaller particles is more critical and costs higher.[3] While both the micro- and nano-silver particles possess excellent properties,[18] it was reported that the silver nanoparticles are potentially harmful to human health.[19] It was also reported that nano-silver is more reactive in an air atmosphere and thus can self-sinter in the absence of coatings around the particles or the solvents in the pastes.[3]

A reliable silver joint possesses a high strength and a dense silver matrix for high mechanical reliability. The strength of sintered micro-silver joints is influenced by the processing parameters such as the sintering temperature, time, and pressure. In general, the shear strength of silver joints is improved by increasing the sintering temperature and time.[14,16,20] The application of sintering pressure and temperature both provide the driving force for reducing the surface energy of the particles during the sintering process. The increase in the sintering temperature and pressure accelerates the diffusion of the silver atoms and the densification process.[3] However, elevated sintering temperature and time increase the manufacturing cost, while excessive sintering pressure leads to crack growth or edge collapse of the chip. Therefore, optimization of the sintering process parameters is necessary to achieve a well-sintered silver joint for SiC power devices while controlling the manufacturing cost.

Extensive work has been carried out to understand and improve the sintering process for silver joints in SiC power devices. Most studies have focused on the sintering of nano-silver joints. Yang et al.[16] studied the effect of various processing parameters (i.e., sintering temperature, pressures, time, thickness of sintered layer, shear rates, and shear temperature) on the shear strength of nano-silver joints in SiC/Cu substrate. Zhang et al.[21] evaluated the reliability of nano-silver joint between SiC and direct bond copper (DBC) with electroless nickel/immersion gold (ENIG). Hong et al.[22] investigated the sintering process for a type of nano-Ag (CT2700R7S; Kyocera Chemical, Japan) for SiC power modules without pressure at 250°C in vacuum and N$_2$ atmosphere. Apart from nano-silver, the use of micro-silver

in joining SiC to DBC was also reported. The sintering process was conducted from 180°C to 350°C for 30 min, without the application of pressure.[23]

To date, the information related to the processing parameters for pressure sintering of micro-silver for SiC power devices is still scarce. In this work, micro-silver pastes were selected as the interconnect material to connect the SiC chip to the DBC substrate using the hot-pressing sintering process. The influence of different sintering parameters (sintering temperature, time, and pressure) on the shear strength of the micro-silver joints was studied. The morphology of the shear fracture surfaces was investigated using scanning electron microscopy coupled with energy-dispersive x-ray spectroscopy (SEM/EDX). The sintering conditions were optimized by performing an orthogonal test. The best combination of sintering temperature, time, and pressure for micro-silver interconnect between SiC and DBC was then proposed. The microstructure of the silver joints sintered under the optimized condition was analyzed. The temperature and hydrostatic pressure distributions during the sintering process using the optimum parameters were also analyzed using the finite element method (FEM). The influence of the processing parameters on the residual shear stress was studied as well. Finally, the residual shear stress analysis obtained from the FEM analysis was correlated with the shear strength obtained from the experiments to show the relationship between the residual shear stress and the shear strength.

Experiment and Simulation

Materials and Methods

In this work, 5 mm × 5 mm × 0.18 mm 4H-SiC chips were bonded to double-sided silver-plated DBC substrates by the hot-pressing sintering process using 90% pure micro-silver pastes from Heraeus. Figure 1 shows the dimensions of the test samples. The back of the SiC chip contains multi-layer coatings of 0.1 μm Ti/0.3 μm Ni/0.4 μm Ag. The dimension of the Cu on each side of the DBC is 29 mm × 13 mm × 0.2 mm, coated with a 0.3 μm-thick Ag layer (electroplated on as-received DBC), while the dimension of the Al$_2$O$_3$ ceramic is 30 mm × 14 mm × 0.5 mm. Two symmetrical SiC chips were bonded to each DBC substrate using micro-silver pastes with particle size of 1–5 μm in flake shape.

Figure 2 shows the process of sample preparation. The DBC substrates were coated with silver to create a better joint with the micro-silver. A 150 μm stencil was used for the stencil printing of the two 5 mm × 5 mm silver pastes. The silver pastes were then preheated at 130°C in flowing N$_2$ gas for 15 min to ensure that the organic solvents in the silver pastes had evaporated completely. The purpose of the
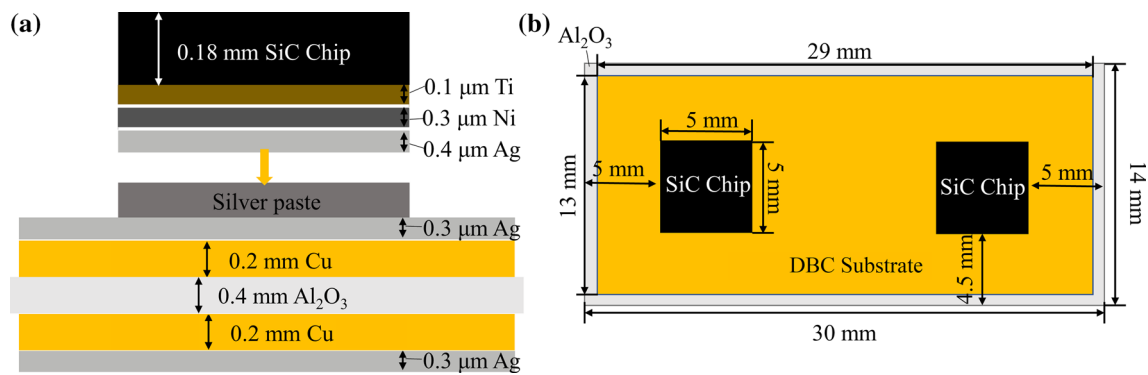
Fig. 1 The dimensions of the test samples (not drawn to scale): (a) front view; (b) top view.
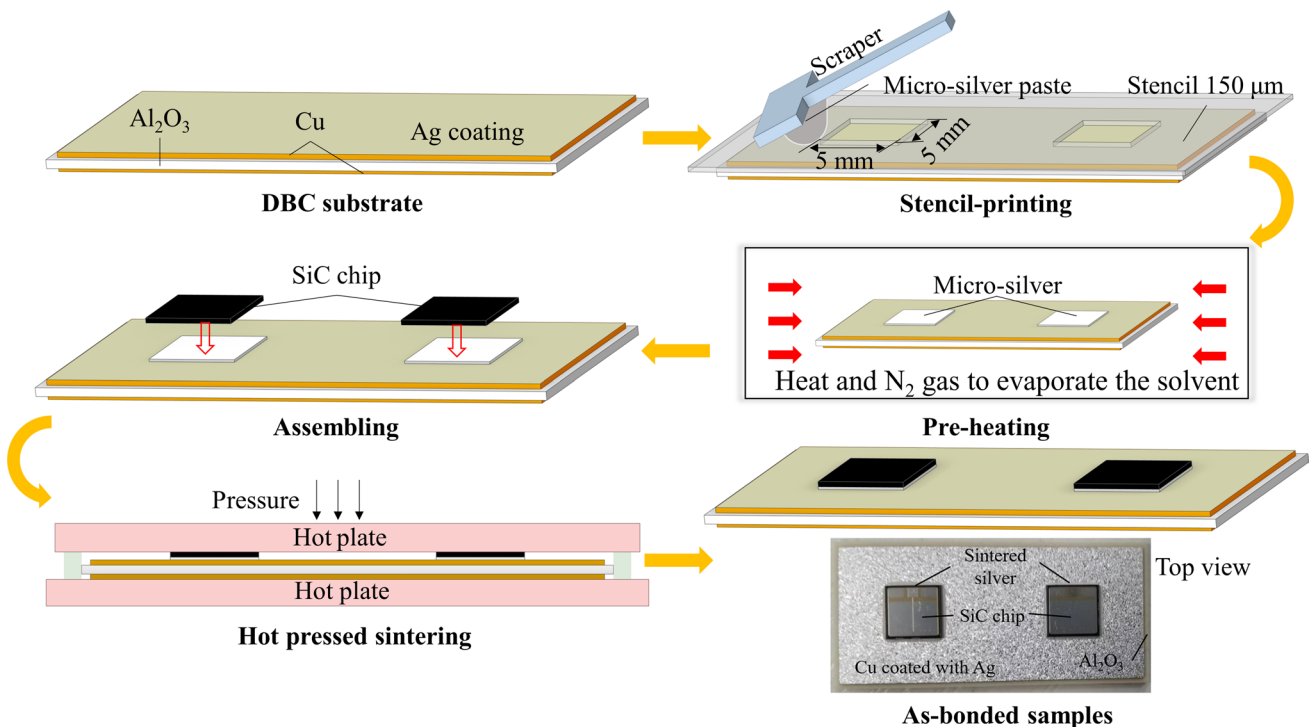

Fig. 2 Sample preparation flowchart of sintered silver joints.

preheating process was to reduce risk of void formation. The temperature profile of the preheating process is depicted in Fig. 3a. The morphology of the silver particles was investigated by SEM/EDX after the preheating process.

Prior to the hot-pressing sintering process, the SiC chips were assembled on top of the micro-silver pastes. The assembled samples were then placed in the sintering furnace and subjected to heat (240–300°C) and pressure (4–16 MPa) for 1–7 min. The curves showing the sintering temperature, time, and pressure during hot-pressing sintering are presented in Fig. 3b.

In order to investigate the effects of the sintering temperature, time, and pressure on the shear strength and fracture sections of the micro-silver joints, single-factor experiments were designed. Table I shows the design of the single-factor experimental conditions. The tests were categorized by C, T, and P which represent the variations in sintering temperature, time, and pressure, respectively. It can be noted that the experimental conditions for tests C4, T3, and P3 are the same. To ensure the reproducibility, three test samples were prepared for each condition.

The sintered silver joints were then subjected to shear tests. The height of the pusher for the shear test was 80 μm,
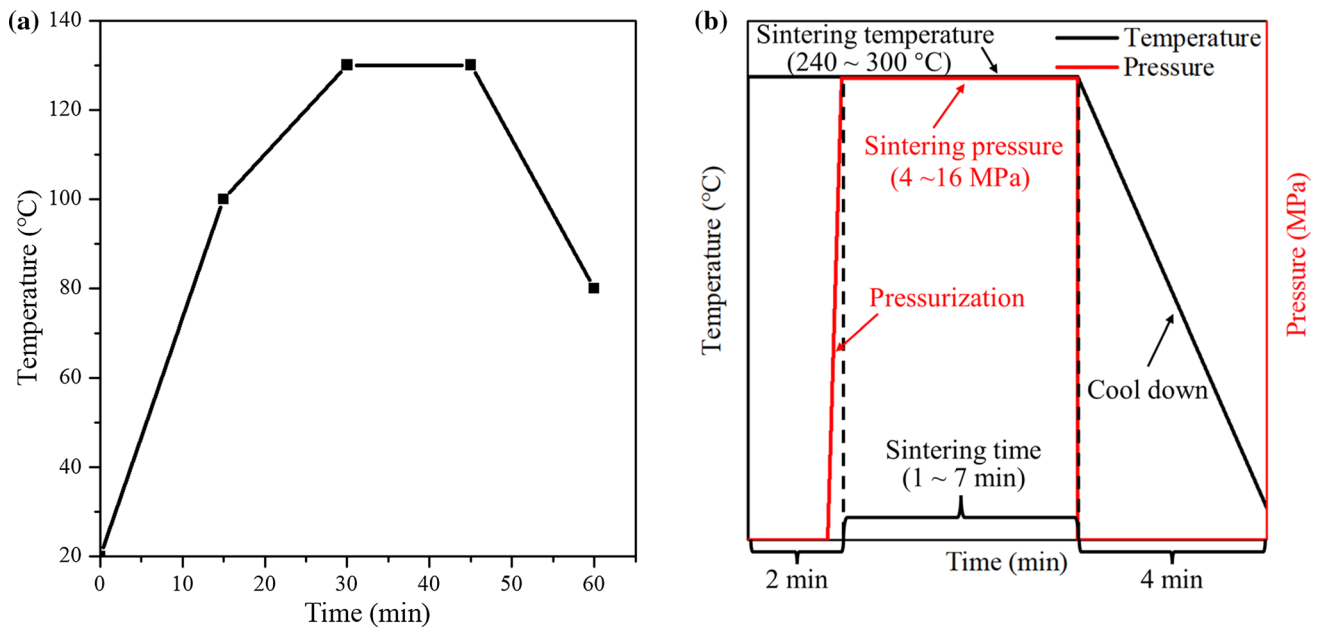
Fig. 3 (a) The curve of the preheating temperature with time; (b) the curve of sintering pressure and temperature with time during hot-pressing sintering.

Table I Single-factor experimental design

Test number	Sintering temperature (°C)	Sintering time (min)	Sintering pressure (MPa)
C1	240	5	12
C2	260	5	12
C3	280	5	12
C4	300	5	12
T1	300	1	12
T2	300	3	12
T3	300	5	12
T4	300	7	12
P1	300	5	4
P2	300	5	8
P3	300	5	12
P4	300	5	16

and the moving speed of the pusher was set at 100 μm/s, as shown in Fig. 4. The shear strength of the silver joints under each condition was determined by averaging the three values obtained from three different samples. The standard deviations of the shear strength of the three samples were calculated and plotted as the error bars in the results. The shear fracture sections of the samples were then observed by SEM/EDX to analyze the fracture mechanism of the silver joints.

In order to optimize the parameters for the micro-silver sintering process, orthogonal tests were designed and conducted after the single-factor experiments, and the optimized

sintering process parameters were obtained by the range analysis. The microstructures of the sintered silver joints and the voids produced under the optimized parameters were then analyzed by SEM/EDX.

Finite Element Method and Model

The sintering process of the micro-silver under the optimum parameters was simulated using FEM in ANSYS to evaluate the temperature and stress distributions. The influence of the temperature and stress distributions on the joint porosity was studied. The influence of different sintering conditions on the residual stress in the sintered joints was investigated as well.

Geometric Model and Material Properties

A geometric model was established according to the real structure and size of the die attach (DA) structure prepared as described in the "Materials and Methods" section. Since the DA structure is symmetric, a simplified 1/4 model (Fig. 5) would be sufficient to reflect the temperature and stress distributions.

The parameters of the material properties used in the FEM analysis are listed in Table II, referring to the work of Yang et al.[24] and Feng et al.[25] It was assumed that both the DBC substrate and SiC chip are elastic and that the parameters remained constant with temperature.

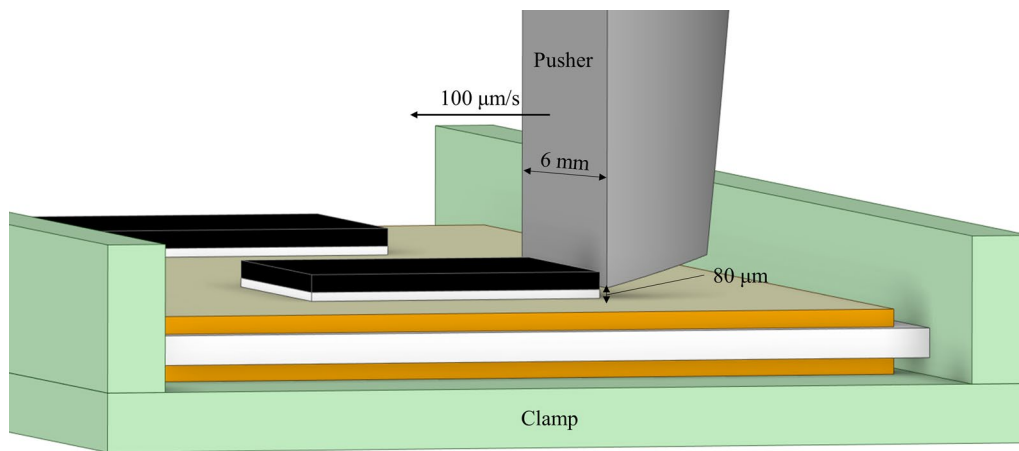The Anand model is commonly used to represent the deformation behavior of solder joints in electronics with

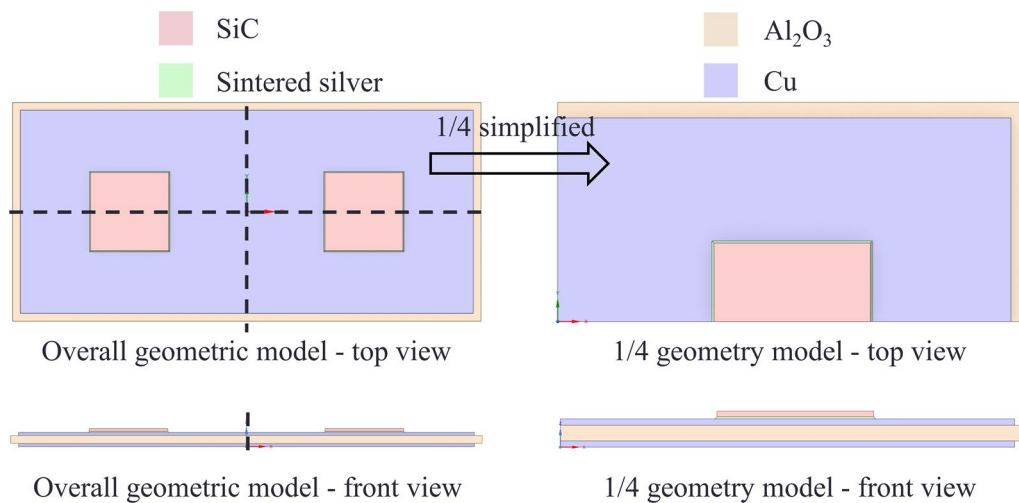**Fig. 4** Shear test diagrammatic drawing of micro-silver joints.

Fig. 5 Geometry model for FEM.

Table II Material properties of SiC and DBC[24,25]

Material	Material properties					
	Density (kg/m^3)	CTE (10^{-6}/K)	Young's modulus (GPa)	Poisson's ratio	Thermal conductivity [W/(m·°C)]	Specific heat [J/(kg·°C)]
SiC	3210	4	420	0.14	353	552
Ag	1049	19.6	4.91	0.37	429	232
Cu	8300	18	110	0.34	401	385
Al$_2$O$_3$	3900	6.8	380	0.27	27	776

viscoplastic deformations. Qian et al.[26] demonstrated that the Anand model could accurately describe the tensile properties of sintered nano-silver. The theories related to the Anand model can be found in the literature.[26,27] Given the viscoplastic behavior of sintered micro-silver, the Anand model was used as the constitutive model in the

FEM analysis of this work. Table III shows the parameters for the sintered silver in the Anand model, referring to the work by Feng et al.[25] and Chen et al.[27]

Boundary Conditions

The boundary conditions were set to ensure that the simulation conditions were as similar to the actual experimental conditions as possible. In the actual sintering process, the transfer of pressure and heat was executed by the heating and

Table III Parameters for sintered silver in the Anand model[25,27]

Model parameter	Content
Viscoplasticity coefficient A (s^{-1})	9.81
Activation energy Q (J/mol)	47,442
Multiplier of stress ξ	12
Strain rate sensitivity of stress m	0.6572
Hardening constant h_0 (MPa)	14,600
Strain rate sensitivity of hardening a	1
Initial deformation resistance S_0 (MPa)	2.93
Coefficient for deformation resistance saturation $\hat{S}$ (MPa)	101.7
Strain rate sensitivity of saturation (deformation resistance) n	0.00326

pressing plate, which was in contact with the top of the SiC chip and the bottom of the DBC substrate. The temperature and the pressure at the top of the SiC chip and the bottom of the DBC substrate were defined as the sintering temperature and pressure in the simulation. A thermal boundary condition was set at the symmetric surfaces (the inner surfaces facing the center of the geometry) to ensure that the heat flux on the symmetric surfaces was zero. The side surfaces (surfaces facing outwards) transferred heat through convective heat transfer with air, and the convective heat transfer coefficient h was 25 W/(m^2·K). Meanwhile, the stress normal to the symmetric surface was assumed to be zero. Finally, a fixed constraint was applied to the centroid of 1/4 of the model.
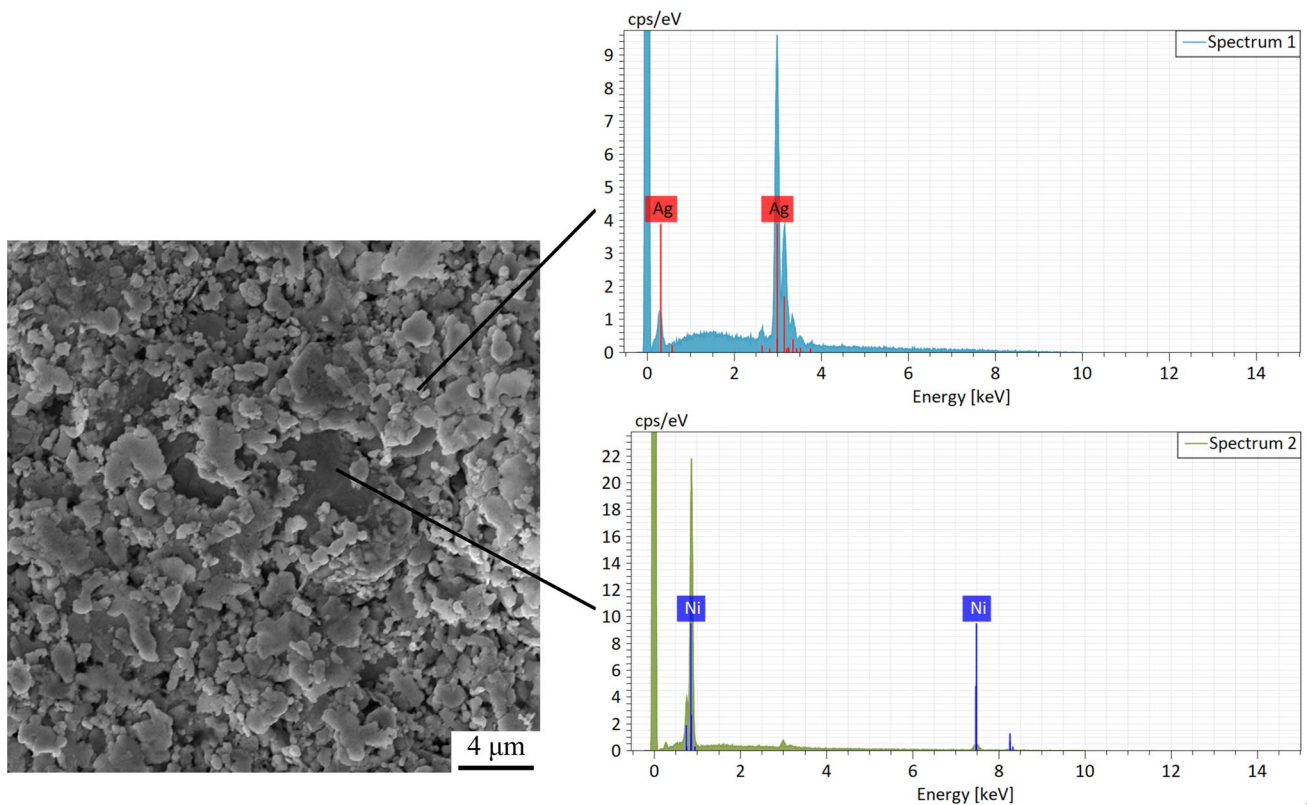
Results and Discussion

Morphology of the Micro-Silver Particles

Figure 6 shows the morphology of the silver particles used in this work. The silver particles are in flake shape, and their diameters are non-uniformly distributed in the range of 1–5 μm. EDX spectra show that apart from Ag, another element, Ni, was also detected. The addition of micro-scale

Fig. 6 Morphology and energy spectra of micro-silver paste after preheating at 130°C for 15 min in N_2 gas.

Ni particles is one of the patented methods in improving the oxidation behavior of silver pastes.[28] It was also reported that the presence of minor Ag-coated Ni particles in Ag pastes could improve the reliability of the pastes by reducing the Young's modulus and modifying the CTE, making the pastes more compatible for the interconnections between SiC chips and substrates.[29]

Effect of Process Parameters on the Shear Performance

Influence of Process Parameters on the Shear Strength

Figure 7 shows the relationship between the shear strength of the micro-silver joints and different processing parameters (i.e., sintering temperatures, times, and pressures). In general, the shear strength of the joints increased with sintering temperature when the sintering time and pressure remained constant at 5 min and 12 MPa. As shown in Fig. 7a, the shear strength increased significantly from 22.08 MPa (240°C) to 40.42 MPa (280°C). However, the rate of increase in the shear strength slowed after 280°C, i.e., the shear strength showed a slight increase of just 0.49 MPa from 280°C to 300°C.

A similar trend can be found from the shear strength–sintering time curve. As shown in Fig. 7b, the shear strength increased greatly from 25.85 MPa to 39.50 MPa with an increase in sintering time from 1 min to 3 min, and then remained almost stable in the range of 39.50 MPa (3 min) to 42.55 MPa (7 min). Although increasing both sintering temperature and time improves the shear strength of the micro-silver joints, there is a limitation. The steepness of the slopes in Fig. 7a and b decreases after reaching a certain extent (280°C and 3 min). This indicates that the shear strength would not show significant improvement with a further increase in temperature and time.

The effect of sintering pressure on the shear strength of the micro-silver joints showed a different trend. With the increase in the sintering pressure, the shear strength of the silver joints first increased and reached a maximum value of 44.39 MPa at sintering pressure of 8 MPa, and then decreased with the pressure beyond that.

It is generally known that an increase in sintering temperature and time increases the shear strength of a sintered silver joint.[16,30] During sintering, silver particles rearrange themselves by sliding and rotating. Diffusion of the silver particles in response to the increases in temperature and sintering time leads to volume shrinkage and densification in the silver joints.[3,16] The increase in the shear strength of the nano- or micro-silver joints with the sintering temperature and time is attributed to the increase in the joint density and the reduction in the porosity within the sintered silver.[30] However, it was also reported that exceeding a certain temperature could result in less improvement or even degradation of the shear performance of a nano-silver layer.[31] The results from this work agree well with the literature. Our findings suggest that sintering at 280°C for 5 min under 12 MPa or sintering at 300°C for 3 min under 12 MPa allowed a complete densification process of micro-silver in flake shape. A further increase in the sintering temperature or time had little benefit on the shear strength.

It was widely reported that increasing the sintering pressure increases the shear strength because it facilitates the densification process of the sintered nano-silver layer.[32] Increasing the sintering pressure could produce silver joints that are sintered "more fully" with a reduced porosity and enhanced thermal and electrical conductivities.[3] However, our findings show that the shear reliability of micro-silver joints degrades with the further increase in sintering pressure above 8 MPa. This means that a good sintering process
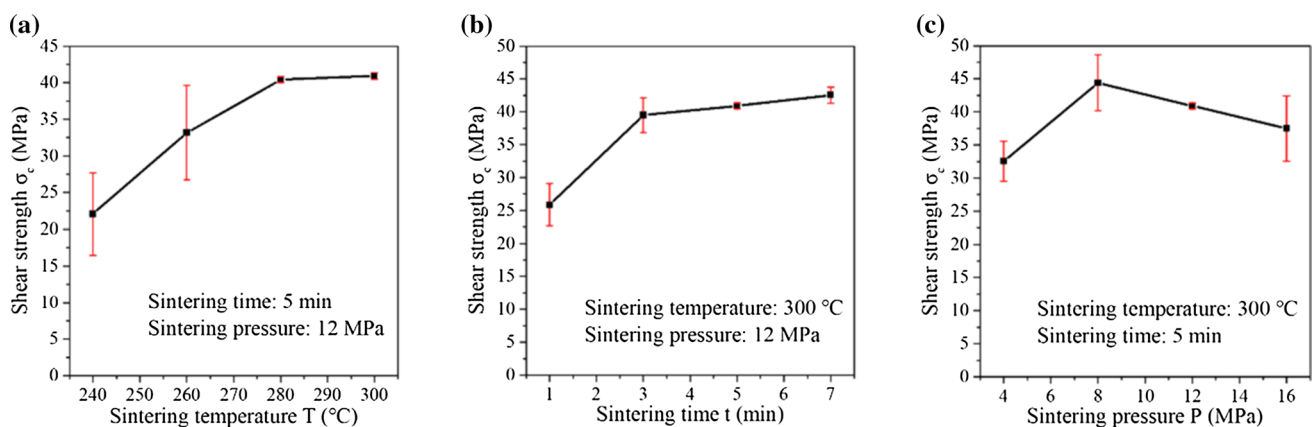
Fig. 7 Influence of (a) sintering temperature, (b) sintering time, and (c) sintering pressure on the shear strength of the sintered micro-silver joints.

occurs under 8 MPa at a sintering temperature of 300°C for 5 min. The depletion in the shear strength with the increase in pressure above 8 MPa could be attributed to the change in the fracture mode and the residual stresses produced, which will be explained in detail in the section "Residual Shear Stress Analysis".

It could be worthwhile to take note that an attempt has been made in this work to produce a sintered micro-silver joint with the sintering pressure of 20 MPa (in 300°C for 5 min). It was found that applying excessive pressure (i.e., ≥ 20 MPa) creates damage to the SiC chips such as breakage and cracks. This in turn affects the functionality of a chip. Therefore, applying a higher sintering pressure does not necessarily improve the quality of the products.

Influence of Process Parameters on the Shear Fracture Surfaces

In order to investigate the effect of processing parameters on the fracture modes, the shear fracture surfaces were characterized by SEM/EDX after the shear tests. The micrographs in Fig. 8a present the typical types of fracture surface of a fractured sintered silver joint. The fracture surface was composed of three different areas, labeled 1, 2, and 3 in Fig. 8a. The magnified micrographs showing their morphologies and the corresponding fracture location are represented by Fig. 8b–g.

The type 1 area appeared to be "whiter" in the SEM micrograph as compared to the rest of the surfaces. The magnified view of the type 1 fracture surface (Fig. 8b) shows obvious dimples that indicate plastic deformations. This type of fracture occurred in the sintered silver matrix with
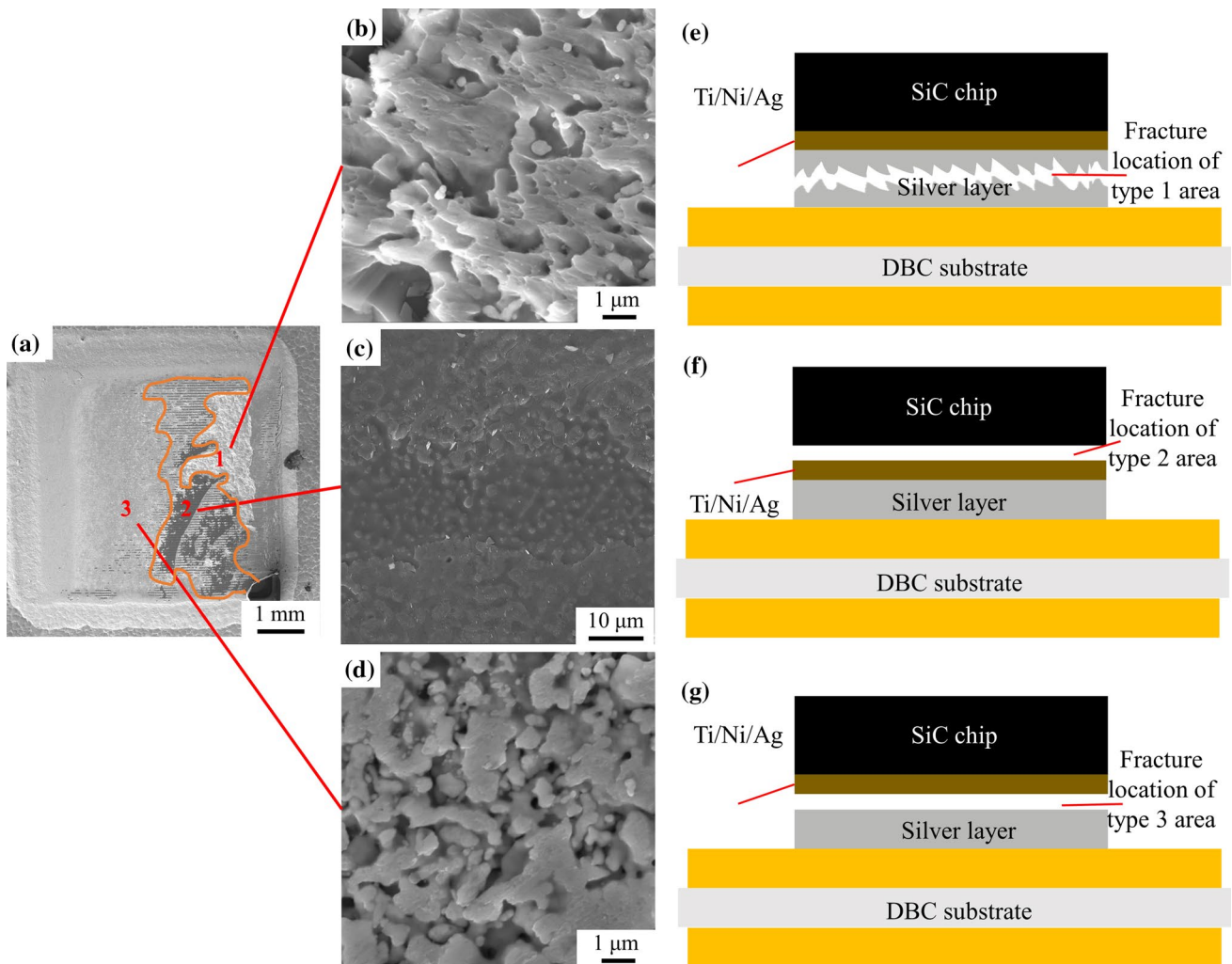
Fig. 8 Typical morphology of different shear fracture surfaces: (a) overview; (b) type 1; (c) type 2; and (d) type 3. Schematic diagram that depicts their corresponding fractured locations in sintered micro-silver: (e) type 1; (f) type 2; and (g) type 3. The processing parameters were 260°C, 5 min, and 12 MPa (C2).

prominent toughness characteristics. Liu et al.[33] and Chew et al.[34] categorized this type of fracture as cohesive fracture mode, where the fracture occurred within the sintered layer.

The type 2 area is shown in Fig. 8c, where a darker material is exposed. EDX analysis (Si 2.18%; Ti 9.85%; Ni 56.07%; and Ag 21.9%) verified that this area consists of the residue of the metal layer coating plated to the back of the SiC chip. The presence of a type 2 surface indicates that the sintered micro-silver layer was not broken during the shear test. It also indicates the excellent bonding between the SiC chip and DBC substrate because the shear strength of the joint is greater than that between the coatings and SiC chips. It can be noted that the bonding strength between the coating and the chip could limit the overall results of shear strength between the SiC chip and DBC substrate.

The fracture surface for the type 3 area is presented in Fig. 8d. Compared to the type 1 area, type 3 is flatter in its appearance. It is suggested to be a brittle fracture based on its morphology. Its morphology revealed that it was the surface of the as-sintered silver, indicating that the silver layer was not well joined to the back of the chip. The presence of type 3 areas indicated the incomplete sintering or unsuccessful joining process in that particular area. It has been categorized as the adhesive break in the literature.[33,34] In general, the observations of type 2 areas are preferred because they represent the formation of good joints between the SiC chip and DBC substrates.

Figure 9 presents the shear fracture sections of the sintered silver joints produced under different sintering parameters, categorized under C (260–300°C), T (1–7 min), and P (4–16 MPa) groups. The effect of different sintering parameters on the types of fracture surfaces produced was investigated. Although all samples contained mixed types of fractured surfaces, it can be observed that the main shear
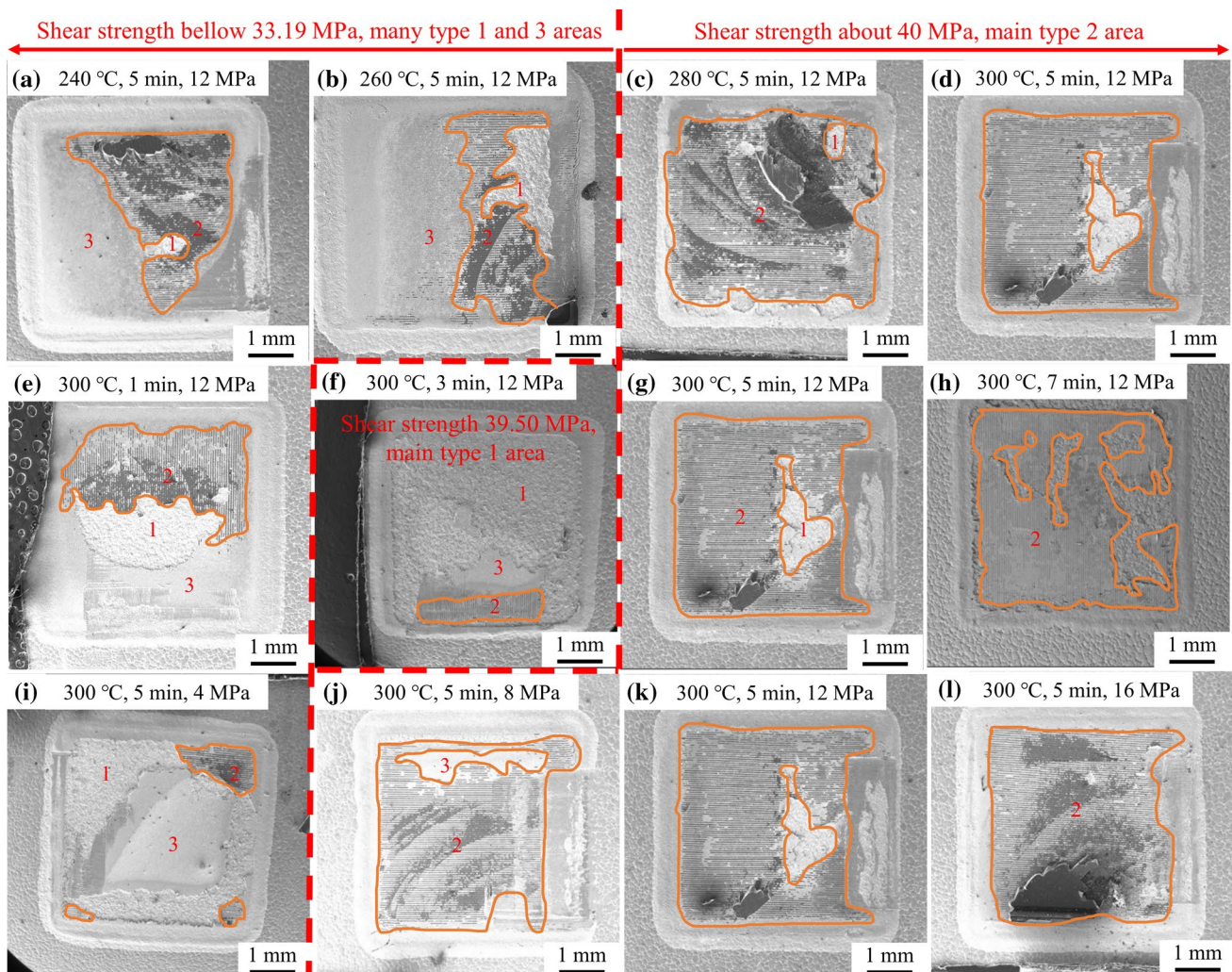
Fig. 9 Shear fracture surfaces of the silver joints sintered at different temperatures, durations, and pressures: (a) C1; (b) C2; (c) C3; (d) C4; (e) T1; (f) T2; (g) T3; (h) T4; (i) P1; (j) P2; (k) P3; (l) P4. The numbers (1, 2, 3) indicate the different types of fracture surface.

fracture types on the right of the red dotted line comprised type 1 and 2 areas, whereas type 1 and 3 areas made up a large part of the fractures to the left of the red dotted line. These observations correlate well with their shear strength.

The fracture surfaces presented at the left to the red dotted line in Fig. 9 are the silver joints with lower shear strength (< 33.19 MPa), whereas those to the right of the red dotted line are fracture surfaces with higher shear strength (~40 MPa). The shear fracture sections in the red dotted box correspond to the micro-silver joints sintered at 300°C and 12 MPa for 3 min and possessed a shear strength of 39.50 MPa (Fig. 9f). It is believed that the shear fracture surfaces to the right of the red dotted line in Fig. 9 are those sintered layers that have undergone a better sintering process. Further increase in the processing parameters would result in a trivial enhancement in the shear strength of the silver joint.

Figure 9a–d show the changes in the shear fracture surfaces of sintered micro-silver with varying sintering temperature from 240°C to 300°C. As shown in Fig. 9a and b, in the shear fracture sections at lower temperatures of 240°C and 260°C (C1 and C2), the excellent joints (type 2 areas) made up a tiny fraction, whereas the incomplete joints (type 3 areas) took up a substantial part. When the sintering temperature was 280°C (Fig. 9c) and above, the excellent joints (type 2 areas) made up the majority of the shear fracture sections, with small number of good joints (type 1 areas). This indicates that high-quality sintered silver joints were produced at a higher temperature, with the sintering time and pressure remaining constant. This could be attributed to the increase in the self-diffusion of the silver atoms between the surface silver coating on DBC substrate and sintered silver layer, and between the sintered silver layer and silver coating on the back of the SiC chip. Based on the shear test results and the observations on the shear fracture surfaces, the range of sintering temperature suitable for the orthogonal test (see the section "Determination of Optimum Sintering Parameters") is determined to be 270–290°C.

The effect of sintering time on the shear fracture surface was investigated as well. As shown in Fig. 9e, with the shortest sintering time, 1 min (T1), although complete joints (represented by type 1 and 2 areas) were visible, more than half of the fracture section exposed showed incomplete sintering, which was represented by type 3 area. The sintering time of 1 min was insufficient for a complete diffusion process. This resulted in a low shear strength of 25.85 MPa. A slight increase in sintering time to 3 min (T2) leads to a significant increase in shear strength to 39.50 MPa. Its fracture surface is indicated by the red dotted box in Fig. 9. The fracture position was mainly at the silver matrix (type 1 areas). The ductile fracture indicates that the sintering process has been partially completed with a sintering time of 3 min (at 300°C and 12 MPa). The strength of the silver matrix of type 1 fracture is almost equal to the joint with a majority of type 2 area of fracture sections. When the sintering time was increased to 5 and 7 min (T3 and T4), the fracture position was concentrated at the interface between SiC and its coating (type 2 area). Some type 1 fractures were also observable. The shear strength of the sintered silver layer increased slightly to 40.91 MPa and 42.55 MPa at 5 and 7 min, respectively. Based on the shear test results and the observations of the shear fracture surfaces, 3–5 min was selected as the sintering time range for the orthogonal test.

Figure 9i–l show the influence of sintering pressure from 4 MPa to 16 MPa on the fracture surfaces. A majority of the fracture surfaces of the micro-silver joint at 4 MPa were types 1 and 3. Increasing the sintering pressure to above 8 MPa (P2–P4) changed the shear fracture surfaces to type 2 with good sintering quality. It is important to note that the further increase in sintering pressure from 8 MPa to 12 MPa and 16 MPa led to the decrease in the shear strength. The decrease in shear strength with sintering pressure could be due to the influence of residual shear stress created during the sintering process, and this will be further discussed in the section "Residual Shear Stress Analysis" The optimum sintering pressure range for the orthogonal test is determined to be 6–10 MPa.

Optimum Parameters for Sintering of Micro-Silver

Determination of Optimum Sintering Parameters

The results obtained from the single-factor experiments reported in the previous sections have narrowed the optimum ranges of the sintering parameters to 270–290°C, 3–5 min, and 6–10 MPa. The optimization of sintering parameters was then carried out by utilizing the orthogonal test $L_9(3^3)$. The optimum processing parameters should ensure low processing costs (i.e., lowest sintering temperature, time, and

Table IV Parameter design and shear strength of orthogonal test samples.

Group number	Sintering temperature (C) (°C)	Sintering time (T) (min)	Sintering pressure (P) (MPa)	Shear strength (MPa)
L1	270	3	6	11.71
L2	270	4	8	18.63
L3	270	5	10	25.39
L4	280	3	8	14.85
L5	280	4	10	30.23
L6	280	5	6	23.87
L7	290	3	10	20.83
L8	290	4	6	25.98
L9	290	5	8	44.31

pressure) without compromising the quality of the micro-silver joints and maintaining excellent shear strength.

The parameters designed for the $L_9(3^3)$ experiment are shown in Table IV. There are three factors involved, including sintering temperature, sintering time, and sintering pressure. The three levels of sintering temperature are level 1 = 270°C, level 2 = 280°C, and level 3 = 290°C. The three levels of sintering time are level 1 = 3 min, level 2 = 4 min, and level 3 = 5 min, and the three levels of sintering pressure are level 1 = 6 MPa, level 2 = 8 MPa, and level 3 = 10 MPa. The shear strength obtained from the orthogonal test is recorded in Table IV. According to the shear fracture test analysis in the section "Effect of Process Parameters on the Shear Performance", the shear strength for samples with excellent joints (type 2 surfaces) is around –40 MPa. Only L_9 group has reached the standard of greater than 40 MPa.

According to the range analysis in Table V, the sintering time has the greatest effect on the shear strength of the silver joints, while sintering pressure has the least effect on the shear strength. The k_i (i = 1, 2, 3) in each row represents the average shear strength of each level. With the increase in the sintering time and temperature, the average shear strength increases significantly ($k_3 > k_2 > k_1$). However, with the increase in sintering pressure, the average shear strength of the silver joints first increased, followed by a slight decrease ($k_3 \approx k_2 > k_1$). The optimal sintering conditions determined based on the orthogonal test are 290°C, 5 min, and 8 MPa.

Interfacial Morphology Under Optimum Parameters

Further inspection into the interface between the SiC chip and DBC substrate was carried out to examine the quality of the micro-silver joint produced under the optimum sintering parameters (290°C, 5 min, 8 MPa). Figures 10 and 11 show the typical microstructures of the cross-sectioned sintered micro-silver joints near the center and the edge of the silver layer, respectively. The sintered silver layer in a lighter appearance was sandwiched between the dark SiC chip and the grayish DBC substrate. Complete bonding regions could be observed from both the upper and lower interfaces of the silver layer. These regions represent the achievement of a good sintering process under these parameters.

The gray layer between the SiC chip and Ag layer was the multilayer coating containing Ti, Ni, and Ag layers. The Ag layers coated on the back of the SiC chip and the top of DBC substrate could hardly be distinguished because they were relatively thinner (~0.3 or –0.4 μm) compared to the micro-silver layer (~40 μm thick).

Other than the sintered silver layer, another darker phase in a bulk form was found distributed homogeneously in the silver matrix. The EDX analysis shows that this phase is composed of Ni. As discussed in the section "Morphology of the Micro-Silver Particles", minor Ni particles were added into the micro-silver paste to enhance its properties, such as CTE and Young's modulus.[29] It was reported that the presence of minor Ni in silver paste could reduce the fatigue cracks by creating a flexible bonding layer. The effect of Ni on the bonding properties is out of the scope of this work and will not be further discussed.

The silver matrix was dense at the center, while pores or voids were observed at the edge (see Fig. 10). From the center to the edge of the silver matrix, the porosity of the silver matrix increased gradually from 2.8% to 16.4%. Although the silver matrix at the edge was porous, neck formation indicating the occurrence of diffusion and densification during the sintering process could be observed.

Compared to the center regions, the porosity of the sintered silver layer at the edge of the SiC chip was higher. The microstructure at the edge of the silver layer is shown in Fig. 11. Similar to that of Fig. 10, the porosity of the silver matrix also decreased gradually from the corner to the center, from 19.8% to 13.0%.

The density distribution of the sintered silver layer was deduced based on the micrographs and drawn in Fig. 12. The areas in which the porosity was greater than 10% were categorized as non-dense regions. The overall density at the center was higher than in the region nearer the edge, with the lowest density (highest porosity) found at the

Table V Range analysis results of orthogonal tests	Shear strength range analysis	Factors		
		Sintering temperature (C)	Sintering time (T)	Sintering pressure (P)
	k_1 (MPa)	18.58	15.80	20.52
	k_2 (MPa)	22.98	24.95	25.93
	k_3 (MPa)	30.37	31.19	25.48
	Range (MPa)	11.79	15.39	5.41
	Order of influence degree	T > C > P		
	Optimal levels	C_3	T_3	P_2
	Optimal combination	290°C 5 min 8 MPa		
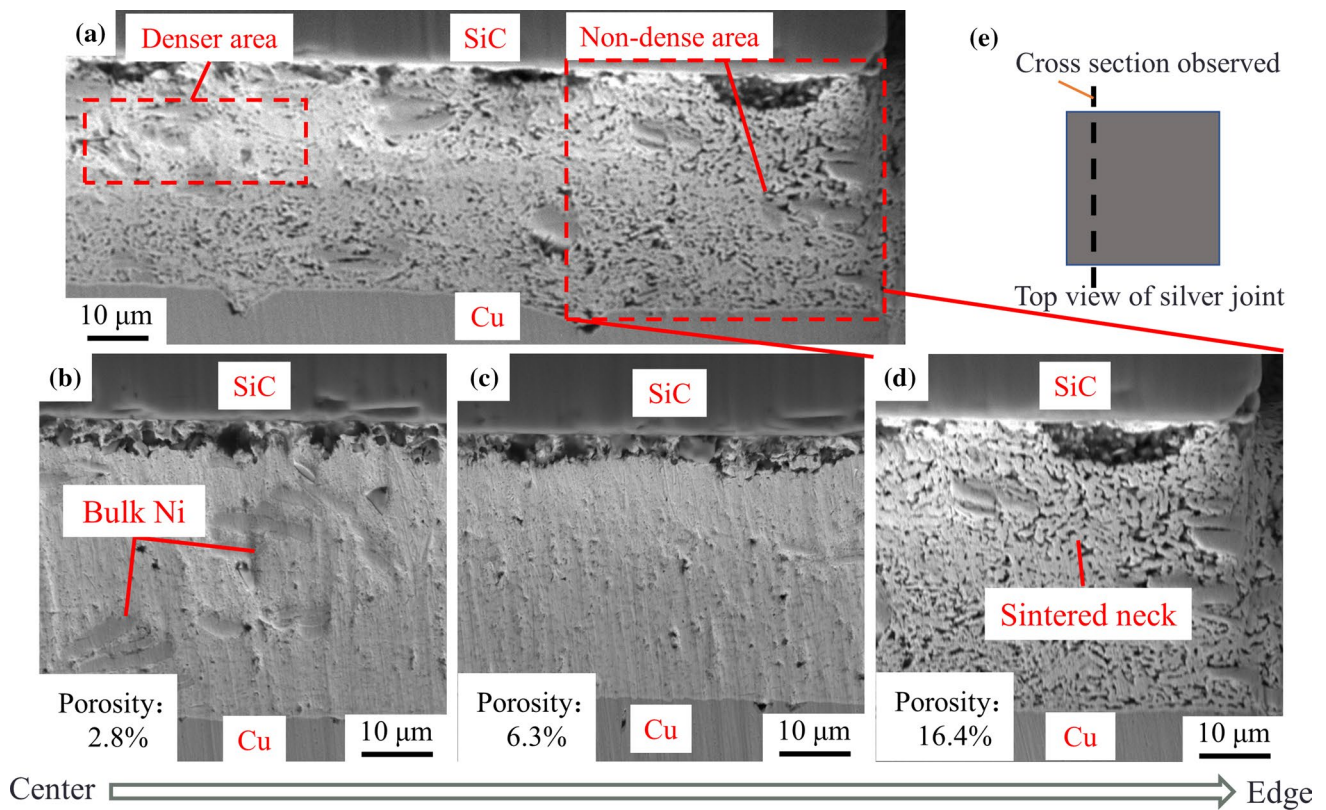
Fig. 10 The microstructure of the silver layer near the center, sintered at 290°C, 5 min, and 8 MPa: (a)–(d) microstructure of the cross section from center to edge; (e) location of the cross section observed.
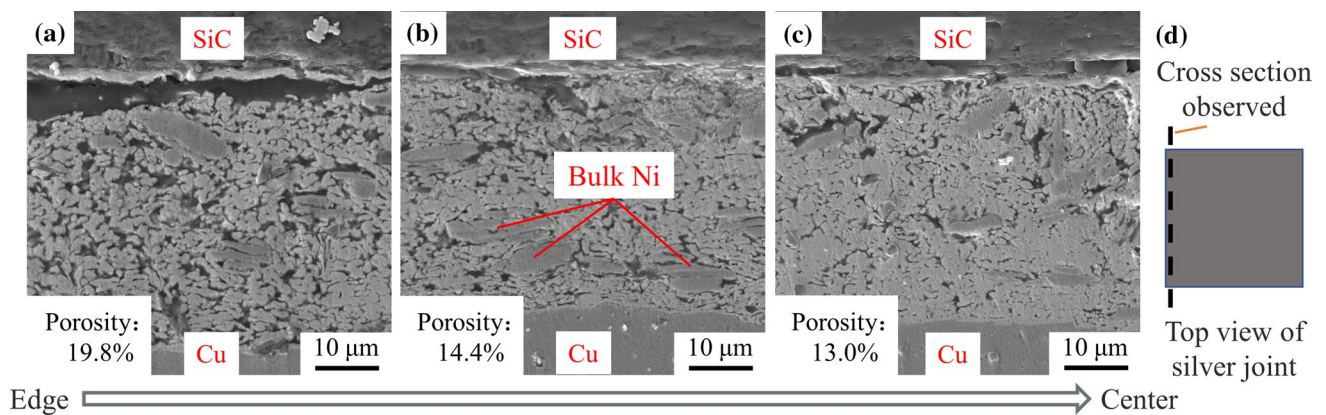
Fig. 11 The microstructure at the edge of the silver layer sintered at 290°C, 5 min, and 8 MPa: (a)–(c) microstructure of the cross section from edge to center; (d) location of the cross section observed.

corner, indicating that the density of the sintered silver layer was uneven. This may be related to the inhomogeneous temperature and pressure distribution at the center, edge, and corner of the silver layer during the sintering process, which will be further elaborated in the following sintering process simulation section.

Shear Performance Under Optimum Parameters

The shear strength of the sintered silver joint produced under the optimum parameters determined in this work (290°C, 8 MPa, 5 min) is 44.31 MPa. The shear strength has far exceeded the required shear strength (12 MPa) specified in

the MIL-STD-883H standard (method no. 2019.8). Table VI compares the shear strength of the silver joints produced under different processing parameters. It is important to note that factors such as the shape of silver particles, die size, die materials, thickness of metallization, and preheating profile also play important roles in determining the shear strength of the joints. Despite the inevitable variances in different works, a brief comparison could be made.

Compared to those sintered without pressure, the micro-silver sintered with pressure can achieve a reasonable shear strength (> 30 MPa) with a shorter sintering time. This is attributed to the decrease in porosity and the increase in density of the silver joints with the application of pressure.[32] The shear performances between micro-silver and nano-silver were compared as well. The shear strength of the micro-silver produced under the same temperature (300°C) in this work is higher than that of nano-silver.

It is essential to note that the shear strength of the micro-silver joint produced in our work has almost reached the maximum value that could be expected from this DA structure. Those samples with a shear strength of greater than 40 MPa possessed mostly type 2 shear fracture surfaces, where the fracture occurred in the metallization coating of the die but not the sintered silver layer. Cross sections

Non-dense region (porosity>10%)
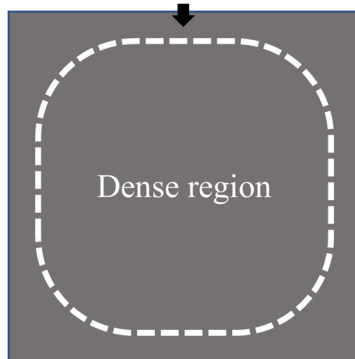
Top view of silver joint

Fig. 12 Schematic diagram of dense and non-dense areas of the sintered silver joint.

showed that the micro-silver generated under these parameters (290°C, 8 MPa, 5 min) formed a good bonding between SiC and DBC with little voids in the silver matrix.

Thermal and Stress Analyses

To further understand the sintering process, the sintering of micro-silver under the optimum parameters (290°C, 5 min, and 8 MPa) was simulated using FEM. The thermal and stress distribution, and the residual stress generated across the DA structure were examined in the simulation.

Thermal Analysis

Figure 13 shows the plots of the minimum, maximum, and average temperature of the DA structure obtained from the simulation of the sintering process. Figure 13a depicts the temperature profile during the first 3.5 s of applying the temperature (300°C), while Fig. 13b shows the temperature change with time of the complete sintering process. The temperature of the overall structure became stable and reached a steady state at 290°C within 1.6 s, as shown in Fig. 13a. Once the upper and lower heating plates contacted the SiC chip and DBC substrate, the temperature of the DA structure increased rapidly. The three curves coincide, indicating the even distribution of temperature across the DA structure (Fig. 13b). The steady state lasted for 7 min (2 min of preheating and 5 min of pressured sintering).

Figure 14 shows the temperature distribution of a quarter of the DA structure at the steady state during sintering. The difference between the highest (290°C) and the lowest (288.37°C) temperatures of the structure during sintering was negligible due to the small size of the DA structure and the superior thermal conductivity of the SiC chip, silver layer, and DBC substrate. The simulation results suggested that the temperature was evenly distributed over the DA structure during sintering at 290°C, and this state could be achieved within 1.6 s when the heat was applied.

Table VI Shear strength of the joints obtained under different processing parameters

| Material	Die and substrate	Sintering type	Sintering temperature (C) (°C)	Sintering time (T) (min)	Sintering pressure (P) (MPa)	Shear strength (MPa)	Reference
Micro-Ag	SiC to DBC	Pressure	290	5	8	44.31	This work
Micro-Ag	Si to Cu	Pressure	230	3	10	–31	34
Micro-Ag	Si to DBC	Non-pressure	250	10	0	–35	35
Micro-Ag	SiC to DBC	Non-pressure	200	30	0	–34	23
Nano-Ag	SiC to DBC	Pressure	300	15	3	–30	21
Nano-Ag	SiC to Cu	Pressure	300	60	7	–38	16

(a)

(b)
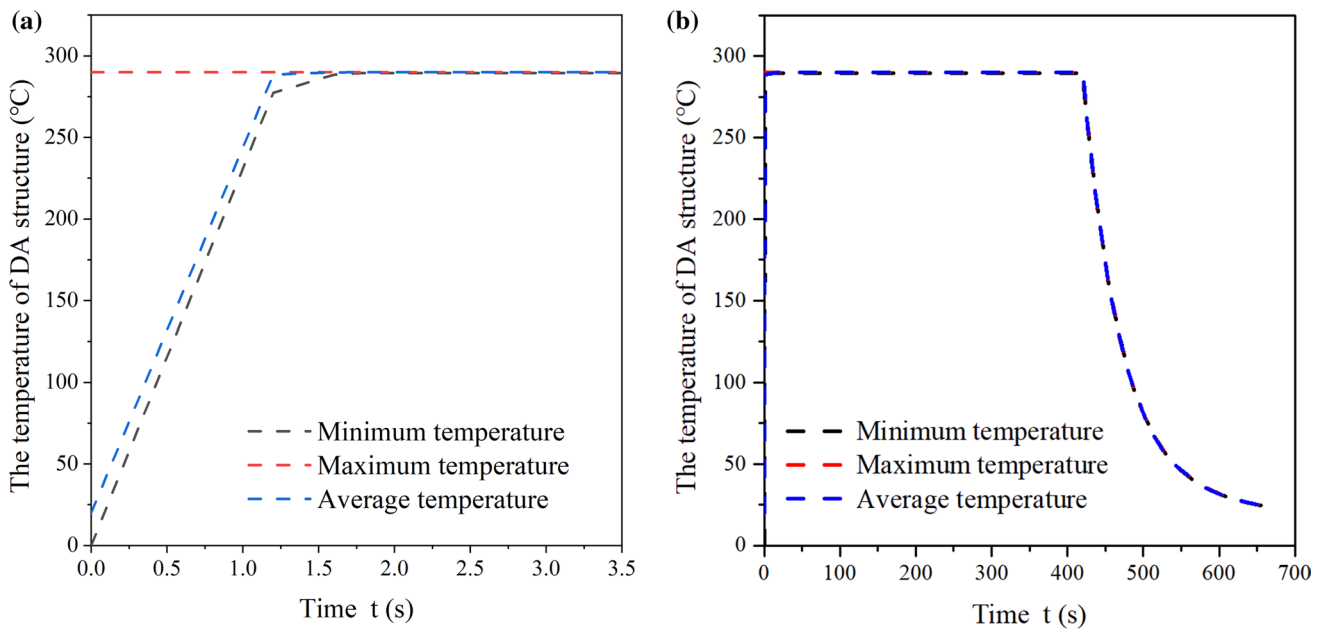
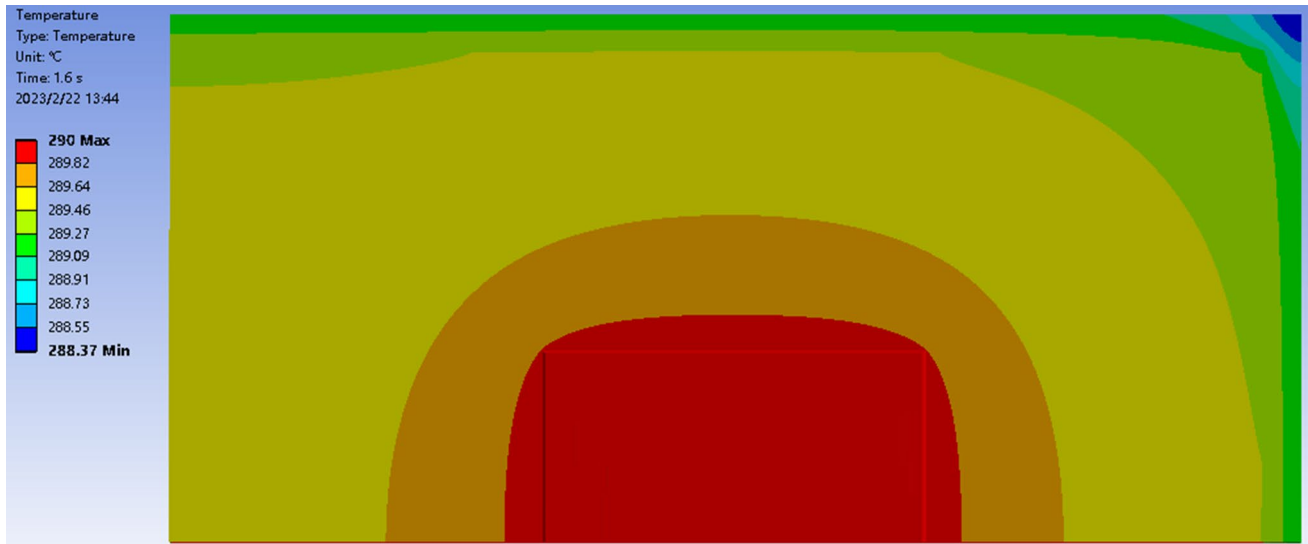Fig. 13 DA structure temperature curves with time during sintering: (a) 0–3.5 s; (b) 0–650 s.

Fig. 14 The temperature distribution diagram (top view) of the simplified 1/4 DA structure when the sintering process reached steady state after 1.6 s.

Stress Analysis

The stress distribution during the sintering process of micro-silver at 290°C, 5 min, and 8 MPa was examined by FEM. According to the mechanics of materials in the x, y, z coordinate system, the stress state of a point in a material $\sigma_{i,j}$ can be described by Eq. 1:[36]

$$\sigma_{ij} = \begin{pmatrix} \sigma_x & \tau_{xy} & \tau_{xz} \\ \tau_{yx} & \sigma_y & \tau_{yz} \\ \tau_{zx} & \tau_{zy} & \sigma_z \end{pmatrix} \tag{1}$$

where σ_x, σ_y, and σ_z represent the stresses along the x, y, and z axis, respectively, while τ_{xy} and τ_{yx} are the stresses of the

xy plane, τ_{xz} and τ_{zx} are the stresses of the xz plane, and τ_{yz} and τ_{zy} are the stresses of the yz plane.

The sintering of micro-silver involves self-diffusion of silver atoms under the influence of temperature and pressure. During the sintering process, the total number of silver atoms remains unchanged. Therefore, the densification process of the silver layer (voids reduction process) can be simplified into an overall volume shrinkage of the silver joint.[3] The change in volume can be expressed by Eq. 2:

$$\theta = \frac{1-2v}{E}\left(\sigma_x + \sigma_y + \sigma_z\right) = 3\left(\frac{1-2v}{E}\right)\sigma_m, \qquad (2)$$

where v is Poisson's ratio, E is the elastic modulus, and σ_m is the hydrostatic pressure, which is the average of the three normal stress components.

The stress tensor can be decomposed into a form as shown in Eq. 3:

$$\sigma_{ij} = \begin{pmatrix} \sigma_x & \tau_{xy} & \tau_{xz} \\ \tau_{yx} & \sigma_y & \tau_{yz} \\ \tau_{zx} & \tau_{zy} & \sigma_z \end{pmatrix} = \sigma_{ij} = \begin{pmatrix} \sigma_x - \sigma_m & \tau_{xy} & \tau_{xz} \\ \tau_{yx} & \sigma_y - \sigma_m & \tau_{yz} \\ \tau_{zx} & \tau_{zy} & \sigma_z - \sigma_m \end{pmatrix} + \begin{pmatrix} \sigma_m & & \\ & \sigma_m & \\ & & \sigma_m \end{pmatrix} \qquad (3)$$

where the first term on the right side of Eq. 3 is the stress deviation tensor, determining the shape change in the material, and the second term on the right side is the stress sphere tensor, determining the volume change in the material. Therefore, the densification process of the silver joint can be related to the hydrostatic pressure in the silver layer.[37]

The minimum, maximum, and average hydrostatic pressures of the silver layer with respect to time in the sintering process, suggested by the simulation results, are shown in Fig. 15. In the initial stage or the heating stage (0–120 s), the average hydrostatic pressure inside the silver joints is approximately 0. At this stage, the stress on the silver joints

had little contribution to the sintering process, including the volume shrinkage, neck formation, and densification process.

Figure 16a shows the hydrostatic pressure distribution in the silver layer at 120 s. The hydrostatic pressure was distributed symmetrically during the sintering process. The hydrostatic pressure was positive at the edge of the silver layer (shown by the red and yellow areas in Fig. 16a), but negative in the center region of the silver layer (shown by blue areas in Fig. 16a). The positive stress represents the tensile stress, while the negative stress represents compressive stress. This explains the higher density of the silver matrix near the center region and the higher porosity near the edges and voids.

In the second stage, the heating and pressuring stage (120–420 s), the hydrostatic pressure in the sintered silver layer decreases rapidly upon the application of 8 MPa and remains stable after 180 s (see Fig. 15). The average hydrostatic pressure is −7.73 MPa, slightly lower than the set sintering pressure (8 MPa). At this stage, the presence of sintering pressure provides the driving force for the sintering process, which enhances the quality of the sintered joint.

The hydrostatic pressure distribution of the sintered silver layer in the second stage, the heating and pressuring stage, is shown in Fig. 16b. The pressure distribution is similar to that of the previous stage: the hydrostatic pressure near the center of the silver layer is less than zero, indicating compressive stress; and the hydrostatic pressure at the edges is more than zero, indicating tensile stress. It is important to note that the difference between the maximum and minimum stresses is large at this stage. Consequently, the silver layer near the center is denser, and the silver layer at the edges has more voids. The results suggested from the simulation correlated well with the experimental findings in the section "Interfacial Morphology Under Optimum Parameters".

In the final stage, the cooling stage (420–660 s), the average hydrostatic pressure increases in response to the removal of the heating and pressuring plate (compressive stress). This promotes the volume expansion of the sintered silver layer. Subsequently, the hydrostatic pressure exists in the sintered silver layer in the form of residual hydrostatic stress of around 10.7 MPa. The presence of residual stress could affect the strength and reliability of the DA structure. However, at this stage, the temperature of the silver layer decreases rapidly, which leads to the rapid decrease in the diffusion rate of the Ag atoms. Thus, the microstructural morphology of sintered silver is little affected.
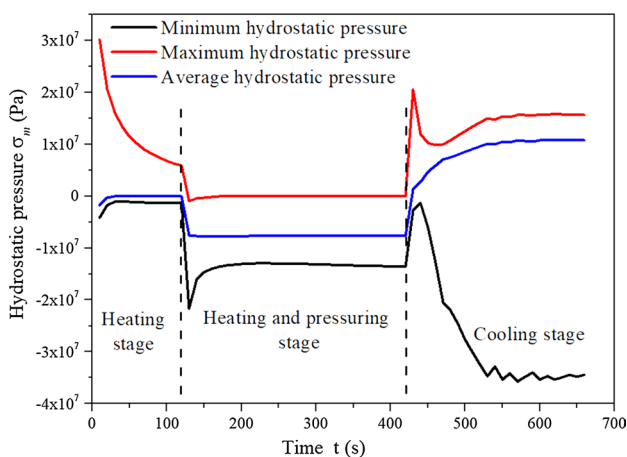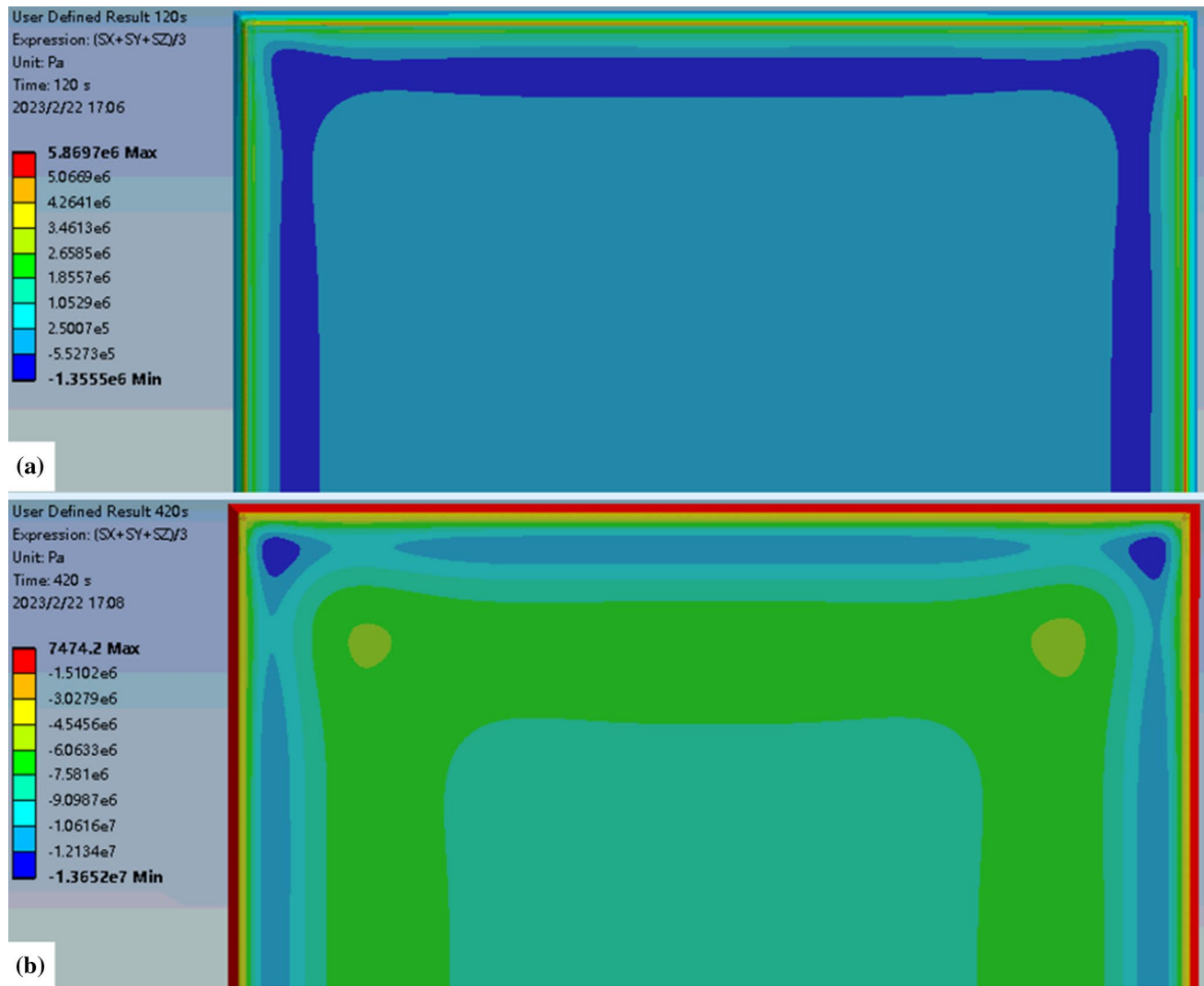

Fig. 15 The curves of hydrostatic pressure of the silver layer over time during sintering.

Fig. 16 Top view of the hydrostatic pressure distribution of sintered silver layer: (a) during the heating stage at 120 s; (b) during the heat and pressure stage at 420 s.

The temperature and pressure distributions in the silver layer during the sintering process play a significant role in the sintering quality (density) in different areas of the silver layer. Simulation results show that the temperature distribution on the silver layer during sintering was uniform. Pressure distribution across the structure during sintering was the main influencing factor on the difference between the density at the edge and at the center of the silver layer.
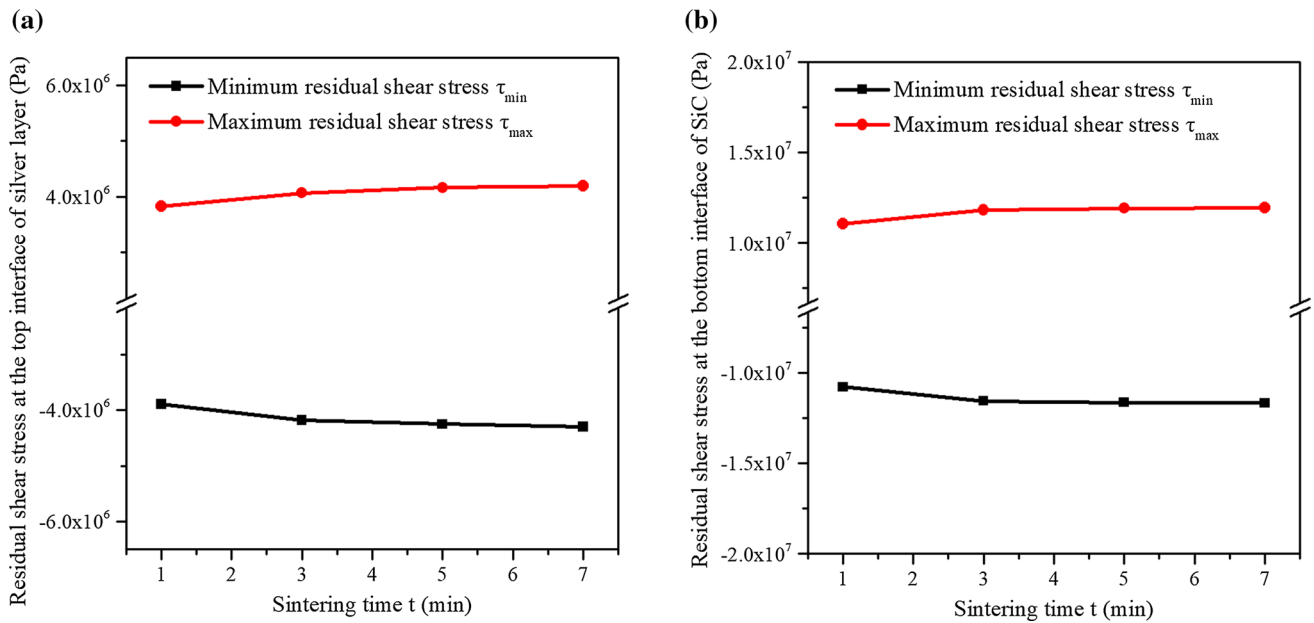
Residual Shear Stress Analysis

The simulation of the pressure distribution across the DA structure suggests that the sintering process can generate residual stresses. Shear strength measures the ability of the DA structure to withstand forces applied parallel to the SiC/Ag/DBC interfaces. The analysis of the shear fracture surfaces (section "Influence of Process Parameters on the Shear Fracture Surfaces") reveals that the shear strength was the highest when most of the fracture occurred within the SiC chip and its coatings. Therefore, the investigation on the residual shear stresses acting in a direction parallel to the SiC chip/silver layer interface was made and correlated with the shear strength of the DA structure. The maximum and minimum residual shear stresses are recorded and plotted as a function of the sintering parameters.

Figure 17 shows the changes in the residual shear stresses at the SiC chip/silver layer interface as a function of sintering temperature. The maximum residual shear stresses of the top interface of the silver layer (4.9–4.2 MPa) and the bottom interface of the SiC chip (13.7–11.9 MPa) decreased gradually with the sintering temperature.
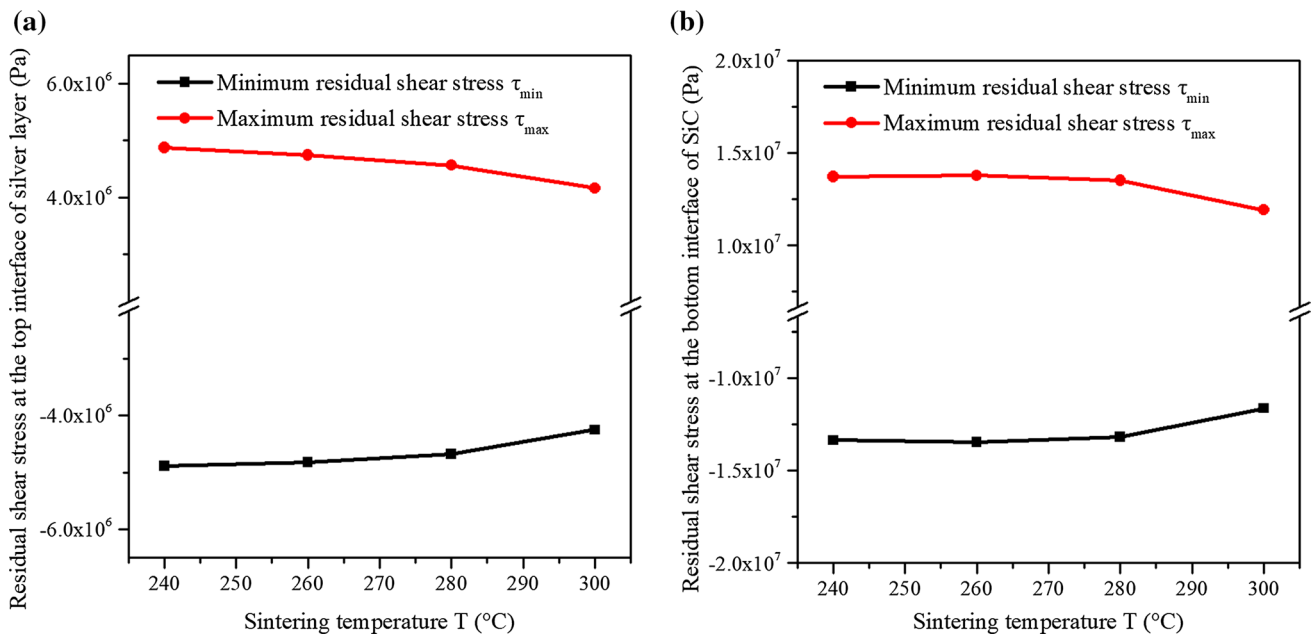
Fig. 17 Curves showing the change in residual shear stress with sintering temperature at the interface between the silver layer and SiC chip: (a) top of the silver layer; (b) bottom of the SiC.
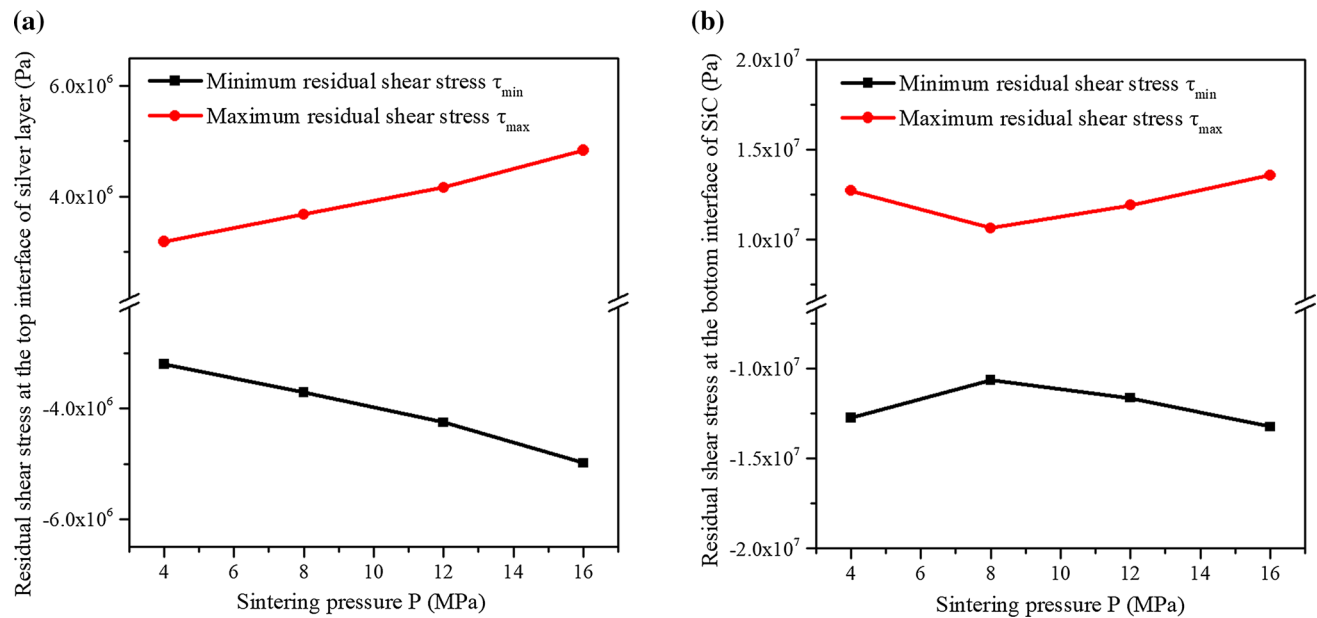

Fig. 18 Curves showing the change in residual shear stress with sintering time at the interface between the silver layer and SiC chip: (a) top of the silver layer; (b) bottom of the SiC.

The changes in residual shear stresses at the interface between the SiC chip and silver layer with respect to sintering time are shown in Fig. 18. The maximum residual shear stresses at both the top interface of the Ag layer and the bottom interface of SiC increased slightly from 1 min to 3 min. The residual shear stresses showed little change with sintering time at 5 min and above. The results indicate that the sintering time has little effect on the residual stresses.

The changes in the residual shear stresses at the interface between the SiC chip and silver layer with respect to sintering pressure suggested by the simulation are shown in Fig. 19. The maximum residual shear stress on the top of the silver layer (Fig. 19a) increased gradually (3.9–5.0 MPa)

(a)

(b)

Fig. 19 Curves showing the change in residual shear stress with sintering pressure at the interface between the silver layer and SiC chip: (a) top of the silver layer; (b) bottom of the SiC.

with the sintering pressure (4–16 MPa). However, the maximum residual shear stress at the bottom of the SiC chip (Fig. 19b) first decreased and then increased with the sintering pressure. The minimum residual stress (10.6 MPa) was generated when the sintering pressure was 8 MPa. A further increase in the sintering pressure results in the increase in the residual shear stress.

The findings from the simulation were compared to those from the findings based on the experiments. It was found that the findings from the simulation agree well with the findings of the shear strength and shear fracture surfaces from the experiments. The shear strength was observed to increase with temperature. This corresponds to the analysis of the shear fracture surfaces (section "Influence of Process Parameters on the Shear Fracture Surfaces"), in which the sintering process of silver layer was more "complete" (more type 2 surfaces) with the increase in temperature because the self-diffusion of silver atoms was more rapid at a higher temperature. Both the more "complete" sintering and the decrease in the residual stress with temperature resulted in an increase in the shear strength with sintering temperature from 240°C to 280°C.

The shear strength first increased with sintering pressure from 4 MPa to 8 MPa and then decreased with the sintering pressure above 8 MPa. Our results suggest that the higher the residual shear stress at the SiC/silver layer interface, the greater the deterioration it could cause on the shear strength of the DA structure.

In short, the simulation results suggest that the sintering temperature and sintering pressure affect the state of the residual shear stress at the SiC chip/sintered silver interface, while the sintering time has little influence on the residual shear stress. The residual shear stress decreases monotonously with the sintering temperature, and first decreases then increases with the sintering pressure. The residual shear stress in turn affects the shear strength of the DA structure.

Conclusions

The effects of various sintering parameters, including the sintering temperature, duration, and pressure, on the shear performance of the micro-silver joint between SiC chips and DBC substrates were investigated. The thermal distribution, stress distribution, and residual stress produced during the sintering process have been simulated using FEM. The findings from the experiment and the simulation were then compared and correlated.

Experimental results showed that the shear strength of the sintered micro-silver increased with both the sintering temperature and time, but first increased and then decreased with sintering pressure. The optimum parameters were determined to be 290°C, 5 min, and 8 MPa, with a promising shear strength of 44.31 MPa. The shear fracture surface morphologies can be classified into three distinct types: type 1, fracture occurred within the silver matrix; type 2, fracture occurred within the SiC chip (chip/coating interface); and type 3, separation occurred at the flat sintered silver interface, indicating poor joints. The samples with more type 2

region possessed higher shear strength. The larger the type 2 region, the better the joint quality.

FEM analysis demonstrated an even temperature distribution during the sintering process using optimized parameters. On the contrary, the pressure was not evenly distributed. This resulted in the higher porosity (>10%) at the edges and corners of the sintered silver layer. The residual stress at the micro-silver/SiC interface first increased then decreased with sintering pressure. The residual stress obtained from FEM analysis correlated well with the shear strength determined from the experiments. The larger the residual shear stress, the lower the shear strength. The increasing residual shear stress that came along with the excessive sintering pressure (> 8 MPa) played an important role in reducing the shear strength.

This work explored the best combination of processing parameters for pressure sintering of micro-silver joints between SiC and DBC that produces promising joints at lower processing cost, which benefits the industry and the consumer. The findings from the characterizations of fractured surfaces and FEM analysis provide a better understanding of the sintering process of micro-silver in SiC packages, which is crucial for the establishment of a reliable joining technology.

References

1. R.T. Yadlapalli, A. Kotapati, R. Kandipati, and C.S. Koritala, A review on energy efficient technologies for electric vehicle applications. *J. Energy Storage.* 50, 104212 (2022).
2. L. Han, L. Liang, Y. Kang, and Y. Qiu, A review of SiC IGBT: models, fabrications, characteristics, and applications. *IEEE Trans. Power Electron.* 36, 2080 (2021).
3. A. Syed-Khaja and J. Franke, Silver Sintering, *CIRP Encyclopedia of Production Engineering*. ed. S. Chatti, and T. Tolio (Berlin: Springer, 2018), p. 1.
4. K.S. Siow, Are sintered silver joints ready for use as interconnect material in microelectronic packaging? *J. Electron. Mater.* 43, 947 (2014).
5. G. Liu, Y. Wu, K. Li, Y. Wang and C. Li, Development of high power SiC devices for rail traction power systems. *J. Cryst. Growth* 507, 442 (2019).
6. E. van Brunt, L. Cheng, M.J. O'Loughlin, J. Richmond, V. Pala, J.W. Palmour, C.W. Tipton, and C. Scozzie, 27 kV, 20 A 4H-SiC n-IGBTs. *Mater. Sci. Forum* 821–823, 847 (2015).
7. S. Piriienko, T. Röser, M. Neuburger, and A. Balakhontsev, Current source gate drivers for 3-phase VSI operated in small-scale wind turbine systems. *Int. J. Electr.* 141, 108160 (2022).
8. H. Luo, N. Baker, F. Iannuzzo, and F. Blaabjerg, Die degradation effect on aging rate in accelerated cycling tests of SiC power MOSFET modules. *Microelectron. Reliab.* 76–77, 415 (2017).
9. L. Yang, Y. Yang, Y. Zhang, F. Xu, J. Qiao, W. Lu, and B. Yu, Microstructure evolution and mechanical properties of the In–Sn–20Cu composite particles TLP bonding solder joints. *Appl. Phys. A* 126, 343 (2020).
10. Y. Bao, A. Wu, H. Shao, Y. Zhao, and G. Zou, Effect of powders on microstructures and mechanical properties for Sn–Ag transient liquid phase bonding in air. *J. Mater. Sci. Mater. Electron.* 29, 10246 (2018).
11. G. Khatibi, A. Betzwar Kotas, and M. Lederer, Effect of aging on mechanical properties of high temperature Pb-rich solder joints. *Microelectron. Reliab.* 85, 1 (2018).
12. Z.X. Zhu, C.C. Li, L.L. Liao, C.K. Liu, and C.R. Kao, Au–Sn bonding material for the assembly of power integrated circuit module. *J. Alloys Compd.* 671, 340 (2016).
13. Y. Gao, S. Takata, C. Chen, S. Nagao, K. Suganuma, A.S. Bahman, and F. Iannuzzo, Reliability analysis of sintered Cu joints for SiC power devices under thermal shock condition. *Microelectron. Reliab.* 100–101, 113456 (2019).
14. W. Zhang, J. Chen, Z. Deng, Z. Liu, Q. Huang, W. Guo, and J. Huang, The pressureless sintering of micron silver paste for electrical connections. *J. Alloys Compd.* 795, 163 (2019).
15. S.T. Chua and K.S. Siow, Microstructural studies and bonding strength of pressureless sintered nano-silver joints on silver, direct bond copper (DBC) and copper substrates aged at 300°C. *J. Alloys Compd.* 687, 486 (2016).
16. H. Yang and W. Zhu, Study on the main influencing factors of shear strength of nano-silver joints. *J. Mater. Res. Technol.* 9, 4133 (2020).
17. L. Yin, F. Yang, X. Bao, W. Xue, Z. Du, X. Wang, J. Cheng, H. Ji, J. Sui, X. Liu, Y. Wang, F. Cao, J. Mao, M. Li, Z. Ren, and Q. Zhang, Low-temperature sintering of Ag nanoparticles for high-performance thermoelectric module design. *Nat. Energy* 8, 665 (2023).
18. C.-H. Tsai, W.-C. Huang, L.M. Chew, W. Schmitt, J. Li, H. Nishikawa, and C.R. Kao, Low-pressure micro-silver sintering with the addition of indium for high-temperature power chips attachment. *J. Mater. Res. Technol.* 15, 4541 (2021).
19. M. Ahamed, M.S. AlSalhi, and M.K.J. Siddiqui, Silver nanoparticle applications and human health. *Clin. Chim. Acta* 411, 1841 (2010).
20. H. Zhang, W. Li, Y. Gao, H. Zhang, J. Jiu, and K. Suganuma, Enhancing low-temperature and pressureless sintering of micron silver paste based on an ether-type solvent. *J. Electron. Mater.* 46, 5201 (2017).
21. H. Zhang, W. Wang, H. Bai, G. Zou, L. Liu, P. Peng, and W. Guo, Microstructural and mechanical evolution of silver sintering die attach for SiC power devices during high temperature applications. *J. Alloys Compd.* 774, 487 (2019).
22. W.S. Hong, M.S. Kim, C. Oh, Y. Joo, Y. Kim, and K.-K. Hong, Pressureless silver sintering of silicon-carbide power modules for electric vehicles. *JOM J. Miner. Metals Mater. Soc.* 72, 889 (2020).
23. C. Chen, Z. Zhang, D. Kim, T. Sasamura, Y. Oda, M.-C. Hsieh, A. Iwaki, A. Suetake, and K. Suganuma, Interface reaction and evolution of micron-sized Ag particles paste joining on electroless Ni-/Pd-/Au-finished DBA and DBC substrates during extreme thermal shock test. *J. Alloys Compd.* 862, 158596 (2021).
24. G. Yang, F. Wu, L. Zhou, X. Luan, X. Zou, H. Liu, Y. Wan, X. Zhang, and B. Wang, Influence of IMC morphology on fatigue stress, strain and life of solder layer between SiC chip and DBC substrate in IGBT under thermal cycling. *22nd International Conference on Electronic Packaging Technology (ICEPT)*, 1 (2021).

25. W. Feng and X. Li, Stress and warping analysis of large area substrate connection in IGBT module package. *Chin. Q. Mech.* 41, 59 (2020).

26. C. Qian, T. Gu, P. Wang, W. Cai, X. Fan, G. Zhang, and J. Fan, Tensile characterization and constitutive modeling of sintered nano-silver particles over a range of strain rates and temperatures. *Microelectron. Reliab.* 132, 114536 (2022).

27. G. Chen, Z.-S. Zhang, Y.-H. Mei, X. Li, D.-J. Yu, L. Wang, and X. Chen, Applying viscoplastic constitutive models to predict ratcheting behavior of sintered nanosilver lap-shear joint. *Mech. Mater.* 72, 61 (2014).

28. L. Wang and Z. Liu, *Conductive silver paste containing micro nickel powder*, C.N.I.P. Administration, Editor. 2015, Anhui Fengyang Decheng Technology Co., Ltd.

29. W. Schmitt, L.M. Chew, and D. Schnee, Silver sinter paste for SiC bonding with improved mechanical properties. *21st European Microelectronics and Packaging Conference (EMPC) & Exhibition*, 1 (2017).

30. R. Khazaka, L. Mendizabal, and D. Henry, Review on joint shear strength of nano-silver pasteand its long-term high temperature reliability. *J. Electron. Mater.* 43, 2459 (2014).

31. T. Wang, X. Chen, G.-Q. Lu, and G.-Y. Lei, Low-temperature sintering with nano-silver paste in die-attached interconnection. *J. Electron. Mater.* 36, 1333 (2007).

32. Y. Liu, H. Zhang, L. Wang, X. Fan, G. Zhang, and F. Sun, Effect of sintering pressure on the porosity and the shear strength of the pressure-assisted silver sintering bonding. *IEEE Trans. Device Mater. Reliab.* 18, 240 (2018).

33. X. Liu, S. Li, J. Fan, J. Jiang, Y. Liu, H. Ye, and G. Zhang, Microstructural evolution, fracture behavior and bonding mechanisms study of copper sintering on bare DBC substrate for SiC power electronics packaging. *J. Mater. Res. Technol.* 19, 1407 (2022).

34. L.M. Chew, W. Schmitt, C. Schwarzer, and J. Nachreiner, Micro-Silver Sinter Paste Developed for Pressure Sintering on Bare Cu Surfaces under Air or Inert Atmosphere. *IEEE 68th Electronic Components and Technology Conference (ECTC)*, 323 (2018).

35. H. Zhang, C. Chen, J. Jiu, S. Nagao, and K. Suganuma, High-temperature reliability of low-temperature and pressureless micron Ag sintered joints for die attachment in high-power device. *J. Mater. Sci.: Mater. Electron.* 29, 8854 (2018).

36. J.L. González-Velázquez, *Mechanical Behavior and Fracture of Engineering Materials* (Cham: Springer, 2020).

37. W.A. Siswanto, M. Arun, I.V. Krasnopevtseva, A. Surendar, and A. Maseleno, A competition between stress triaxiality and joule heating on microstructure evolution and degradation of SnAgCu solder joints. *J. Manuf. Process.* 54, 221 (2020).